Theoretical analysis of the wavelength tuning characteristics in a tunable ECDL based on a s-AFPF

Xiao Xiao (肖 啸)[1*], Yuanfu Lu (鲁远甫)[2,3], Fengqi Yu (于峰崎)[1], and Lei Jin (金 雷)[2,3]

[1]*Research Center for Integrated Electronics, Shenzhen Institutes of Advanced Technology, Chinese Academy of Sciences, Shenzhen 518055, China*

[2]*Research Center for Biophotonics, Institute of Biomedical and Heath Engineering, Shenzhen Institutes of Advanced Technology, Chinese Academy of Sciences, Shenzhen 518055, China*

[3]*Key Lab for Biomedical Informatics and Health Engineering, Shenzen Institute of Advanced Technology, Chinese Academy of Sciences, Shenzhen 518055, China*

[*]*Corresponding author: xiao.xiao@siat.ac.cn*

Received December 31, 2011; accepted February 23, 2012; posted online June 20, 2012

The single cavity all-dielectric thin film Fabry-Perot filter (s-AFPF) is investigated in this letter as a means of tuning the wavelength in an external cavity diode laser (ECDL), and the means of limiting longitudinal mode hopping is also investigated. When a TE or TM plane wave irradiates a s-AFPF, a quasi-linear relationship is found in a certain wavelength range between the optical intensity peak-transmittance wavelength of s-AFPF and the cosine value of plane wave incident angle at s-AFPF. Based on this feature, we propose and investigate a configuration with a s-AFPF in a tunable ECDL. By theoretical calculation, a mode-hop-free wavelength tuning range of ∼5 nm around 1 550 nm is achieved. The ECDL can be used in the application of environmental monitoring, atomic and molecular laser spectroscopy research, precise measurements, and so on.

OCIS codes: 140.2020, 140.3600, 310.6860.
doi: 10.3788/COL201210.S11411.

Tunable external cavity diode lasers (ECDLs) are playing an increasingly important role in coherent optical telecommunications, atomic and molecular laser spectroscopy, precise measurements, and environmental monitors[1]. Currently, two principal configurations in tunable ECDLs are the Littrow configuration[2−7] and the Littman–Metcalf configuration[8−11] and in both the dispersive element is a bulk diffraction grating. In addition, there are also other external cavity configurations which contain different kinds of dispersive elements such as Fabry–Perot etalon[12,13], acousto-optic filter[14,15], electro-optic filter[16,17], as well as others.

The ECDL based on the Fabry–Perot etalon, however, is not as popular as either the Littrow configuration or the Littman–Metcalf configuration. A considerable reason is that the performance of the air-spaced etalon is not good enough and it is hard for the etalon to get a simple but effective tuning mechanism which can make the etalon pass band center wavelength have a synchronous variation with an external cavity longitudinal mode wavelength. As the development of thin film optics, we can replace the air-spaced etalon with a high-performance solid etalon which is manufactured with thin film coating technology. In this letter, we propose a tunable ECDL configuration based on a single cavity, all-dielectric, thin film Fabry-Perot filter (s-AFPF), which is exactly a high-performance solid etalon manufactured with thin film coating technology. By theoretical calculation, we show the tunable ECDL is mode-hop-free over about a 5-nm wavelength range centered at about 1 550 nm.

The membrane structure of a s-AFPF is shown in Fig. 1. It consists of one spacer layer and two symmetrical reflectors. The spacer layer is a half-wave layer, and the two symmetrical reflectors are composed of alternate quarter-wave layers. The detailed membrane structure of a s-AFPF can be divided into two types according to its spacer layer: $(HL)^P$H-2L-H$(LH)^P$ or $(HL)^P$-2H-$(LH)^P$, as indicated in Fig. 2. "H" represents a high-index dielectric medium and "L" represents a low-index dielectric medium, both with an optical thickness of a quarter-wave. From Fig. 2, we can see the "H" layer and "L" layer alternate anywhere except in the spacer layer. In the spacer layer, the medium consists of either two "H" layers or two "L" layers[18]. We use the term "P-value" to indicate exponent P. In an actual manufacturing process, the membrane structure of a s-AFPF is usually deposited on a substrate, which is some type of glass.

Fig. 1. Membrane structure of a s-AFPF.

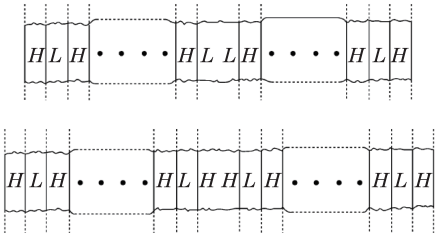

Fig. 2. Two basic types of s-AFPF.

On the opposite side of the substrate, an anti-reflective (AR) coating is deposited to prevent multi-beam interference occurring in the substrate. Therefore, the actual design structure of a s-AFPF is either air|$(HL)^P$H-2L-H$(LH)^P$|glass or air|$(HL)^P$-2H-$(LH)^P$|glass.

For the investigation in this letter, we assume the design structure of the s-AFPF is air|$(HL)^P$H-2L-H$(LH)^P$|glass, among which the "H" layer represents high-index dielectric medium Ta_2O_5 with a refractive index of 2.06, the "L" layer represents low-index dielectric medium SiO_2 with a refractive index of 1.46, the "glass" represents substrate medium K9 glass with a refractive index of 1.5168, we do not consider the dispersion of any refractive material because of the relatively small wavelength band and the low dispersion for these refractive materials around 1 550 nm. We also assume the physical thickness of "H" layer, "L" layer, and "glass" substrate are 193.57 nm, 273.12 nm, and 2 mm, respectively; the "P-value" in air|$(HL)^P$H-2L-H$(LH)^P$|glass is 7. Then, consider the configuration in Fig. 3, an incident plane wave at the s-AFPF with incident angle of θ is shown. When the s-AFPF rotates around a pivot point, θ will change continuously.

By using the characteristic matrix method[18], we can plot the optical intensity transmittance curve of the s-AFPF mentioned above for the TE and TM plane waves, as indicated in Fig. 4. At an incident angle of 0°, there are two identical extremely narrow transmission bands of the s-AFPF for the TE and TM plane waves. As the

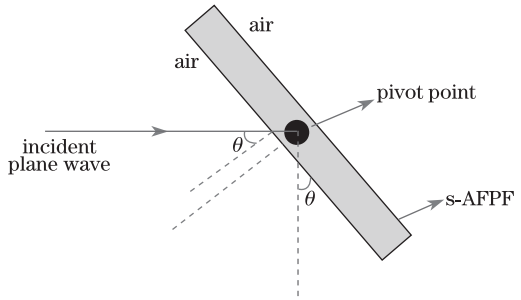

Fig. 3. Two basic types of s-AFPF.

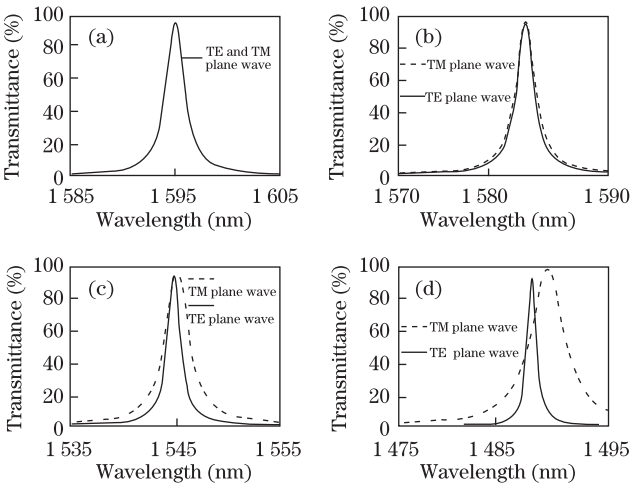

Fig. 4. Extremely narrow transmission bands of the s-AFPF air|$(HL)^7$H-2L-H$(LH)^7$|glass for both TE and TM plane waves at the incident angles of (a) 0°, (b) 12°, (c) 24°, and (d) 36°.

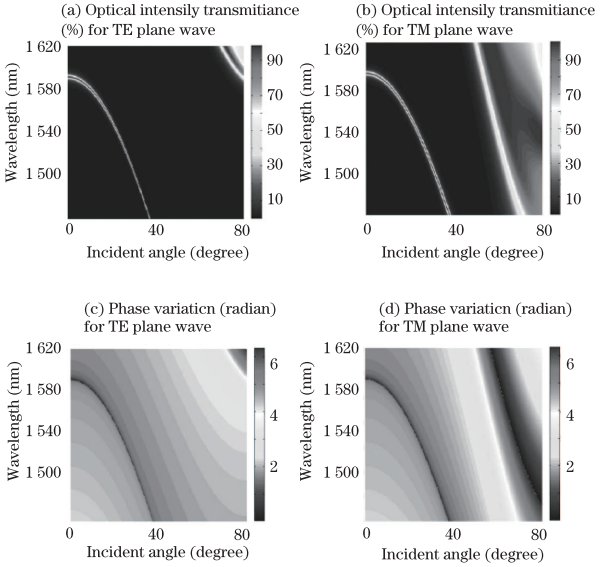

Fig. 5. Distribution of optical intensity transmittance and phase variation as a function of wavelength versus incident angle for TE and TM plane waves, as they pass through the s-AFPF air|$(HL)^7$H-2L-H$(LH)^7$|glass.

incident angle θ increases from 0° to 36°, the TE and TM curves separate gradually. We can control the shift of transmission band center for either TE or TM plane wave by rotating the s-AFPF around a pivot point.

Figure 5 presents the distribution of optical intensity transmittance and phase variation as a function of wavelength versus incident angle for TE and TM plane waves, as they pass through air|$(HL)^7$H-2L-H$(LH)^7$|glass. The optical intensity peak-transmittance wavelength follows a quasi-parabolic curve versus incident angle. Figure 6 shows the relationship between optical intensity peak-transmittance wavelength and the cosine value of the incident angle for TE and TM plane waves. We note the optical intensity peak-transmittance wavelength follows a quasi-linear curve versus the cosine value of the incident angle for both TE and TM plane waves. This quasi-linear property with respect to the cosine value of the incident angle suggested to us a configuration that might have special advantages.

The schematic configuration of the tunable ECDL is shown in Fig. 7. A circular s-AFPF with the design structure of air|$(HL)^7$H-2L-H$(LH)^7$|glass is inserted into the tunable ECDL external cavity, and its diameter is 20 mm; the s-AFPF is vertical to the horizontal plane, but not vertical to the optical axis; it can self-rotate around its central pivot point. The light source in this tunable ECDL is a special laser diode called reflective semiconductor optical amplifier (RSOA, IPSAD1501-3500); on its one side, a high-reflective (HR) thin film coating with a reflectivity of about 90% is deposited; on its other side, an AR thin film coating with a reflectivity less than 0.01% is deposited; the RSOA light will be emitted from its AR coated side, and the collimating lens is also AR coated; the center wavelength of the RSOA light is 1 550 nm, and its 3-dB bandwidth is 60 nm; the small signal gain at peak wavelength of the RSOA is 25 dB, and the threshold current of the RSOA is 15 mA; the output power of the RSOA is typically 2 mW, and its

polarization dependent gain is 12 dB; the operation temperature of the RSOA is always maintained to 25 °C by thermoelectric cooler (TEC). As the polarization dependent gain of the RSOA is 12 dB, its output is mainly TE polarized light (vertical to the horizontal plane), as well as a small amount of TM polarized light (parallel to the horizontal plane). To ensure the output of the tunable ECDL is purely TE polarized light, we insert a circular Brewster window film into the ECDL external cavity, so as to let TE polarized light pass through and TM polarized light be reflected away. The Brewster window film is made of K9 glass without thin film coating; it has a diameter of 20 mm and a physical thickness of 2 mm; the intersecting line of the Brewster window film plane and the horizontal plane is vertical to the optical axis; the Brewster window film plane has a 33.4° angle with the horizontal plane, which can make the RSOA light beam irradiated on the window film at the incident angle of Brewster angle (56.6°). There are two identical circular plane totally reflecting mirrors in the configuration of the tunable ECDL; the reflectivity of them are both 100% when the RSOA light beam is irradiated on them at the incident angle of 45°. There is also a circular plano-concave partially reflecting mirror positioned in the tunable ECDL configuration, and it is vertical to the optical axis; it is made of K9 glass, and has a diameter of 25.4 mm; the curvature radius of its concave surface is 500 mm; a partially-reflective (PR) thin film coating is deposited on its concave surface while an AR coating is deposited on its plane surface.

So, the HR coated side of the RSOA and the concave surface of the plano-concave partially reflecting mirror form the resonator of the tunable ECDL. According to the principles of laser resonator, the external cavity longitudinal mode wavelength changes linearly with change in the optical path length, becoming shorter with decreasing optical path length. However, with greater cavity length, the free spectral range (FSR) of the longitudinal modes decreases, so a long ECDL has a high spectral density of modes. Having many longitudinal modes under the gain width will lead to multi-longitudinal mode output or the laser hopping between modes—creating undesirable performance. In order to filter out the unwanted longitudinal modes, we inserted a s-AFPF discussed above into the external cavity and used its narrow spectral band to reject all but the single desired longitudinal mode.

Meantime, for TE polarized light, Fig. 6 shows that the optical intensity peak-transmittance wavelength of the s-AFPF also changes in a quasi-linear fashion such that the wavelength decreases linearly with the cosine value of increasing θ (TE wave incident angle at s-AFPF) in a certain wavelength range around 1 550 nm. Hence, if the decrease in optical path length and the cosine value of θ can appear simultaneously, and by a proper design of configuration, these two effects may be made to compensate each other to create a substantial mode-hop-free spectral band.

In Fig. 7, the tunable ECDL configuration uses a single actuator to control both the external cavity length and the light beam incident angle at s-AFPF. We assume the initial position of the actuator is where the light beam incident angle at s-AFPF is zero. For forward movement of the actuator from the initial position, the external cavity length decreases and the wavelength of a single longitudinal mode shortens in linear fashion. Meantime, as the actuator pushes forward against the wheel, it drives the s-AFPF to self-rotate counterclockwise around the pivot point, so as to drive the light beam incident angle at s-AFPF to larger values, the cosine of angle to smaller values, and the optical intensity peak-transmittance wavelength of s-AFPF to decrease in quasi-linear fashion. If the length of the pivot point center to the wheel center is set properly for the s-AFPF above, the optical intensity peak-transmittance wavelength of s-AFPF and the wavelength of a given external cavity longitudinal mode may be made to match rather well over a significant range achieving mode-hop-free performance.

For simplicity of analysis in this letter, we regard the collimated laser beam in Fig. 7 as a plane wave. Then, the incident light wave at s-AFPF is now a TE plane wave. For a TE plane wave, we need to consider whether there is a synchronous variation between the pass band center wavelength of s-AFPF and the wavelength of an external cavity longitudinal mode during the process of actuator translation from its initial position.

If we calculate the fractional (longitudinal) mode number of the pass band center wavelength of s-AFPF during the process of actuator translation, we can find which external cavity longitudinal mode will have a synchronous wavelength variation with s-AFPF pass band center wavelength. When the actuator pushes forward from its initial position, the incident angle at s-AFPF and external cavity optical path will change simultaneously. Let the actuator displacement from the initial position be x, the physical thickness of s-AFPF substrate be h, the refractive index of s-AFPF substrate be n, the distance between the pivot point and the wheel be L. In

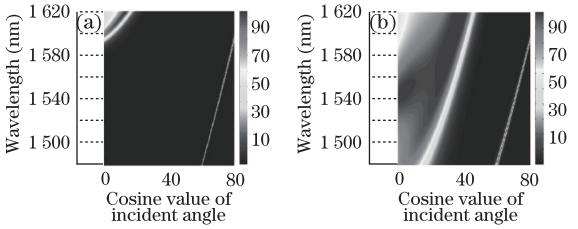

Fig. 6. Distribution of optical intensity transmittance as a function of wavelength versus the cosine value of the incident angle for (a) TE and (b) TM plane waves, as they pass through the s-AFPF air|(HL)^{7}H-2L-H(LH)^7|glass.

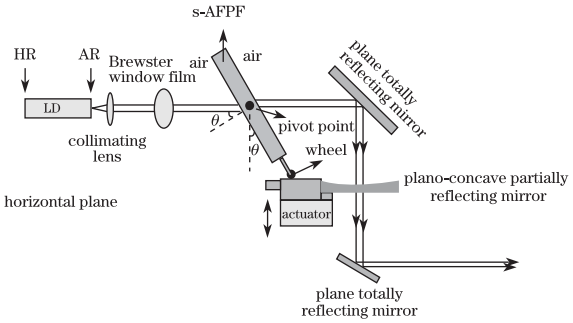

Fig. 7. External cavity configuration to maintain a single longitudinal mode as the s-AFPF is rotated.

the meantime, let the pass band center wavelength of s-AFPF and the round trip optical path length of external cavity be $w_s(x)$ and OPL(x). We define a fractional mode number $m_s(x)$ which is the ratio of OPL(x) to $w_s(x)$:

$$m_s(x) = \frac{\mathrm{OPL}(x)}{w_s(x)}. \tag{1}$$

The fractional mode number $m_s(x)$ is simply a real number representing where the mode should be for maximum s-AFPF transmission. If OPL(x) is made to track $w_s(x)$ closely as x varies, $m_s(x)$ will be nearly constant and an ECDL running on $w_s(x)$ may be mode-hop-free over a relatively wide range.

Figure 8 presents the details that affect the round trip optical path length of the external cavity as the actuator pushes forward from the initial position. In Fig. 8, let the external cavity optical path difference between initial position "position 1" and current position "position 2" be OPD. We have

$$\mathrm{OPD} = 2\left\{(a+nh+b_1+b_2)-\left[(a-h_1)+\frac{nh}{\cos\alpha}+y_1+y_2\right]\right\}. \tag{2}$$

We also have

$$a+h+b_1+b_2-x = (a-h_1)+\frac{h*\cos(\theta-\alpha)}{\cos\alpha}+y_1+y_2. \tag{3}$$

We substitute Eqs. (3) into (2) to eliminate y_1+y_2 and get

$$\mathrm{OPD} = 2\left[nh-\frac{nh}{\cos\alpha}-h+x+\frac{h*\cos(\theta-\alpha)}{\cos\alpha}\right]. \tag{4}$$

From Fig. 8, we know

$$\cos\alpha = \sqrt{1-(\sin\alpha)^2} = \sqrt{1-(\frac{\sin\theta}{n})^2} = \frac{\sqrt{n^2-1+(\cos\theta)^2}}{n}, \tag{5}$$

$$\cos\theta = \frac{L-x}{L}, \tag{6}$$

so, we have:

$$\cos\alpha = \frac{\sqrt{n^2L^2+x^2-2xL}}{nL}, \tag{7}$$

$$\cos(\theta-\alpha) = \frac{2xL-x^2+(L-x)\sqrt{n^2L^2+x^2-2xL}}{nL^2}. \tag{8}$$

Substitute Eqs. (7) and (8) into (4) to get the change in external cavity round trip optical path length, OPD(x):

$$\mathrm{OPD}(x) = 2\left[nh-\frac{n^2hL}{\sqrt{n^2L^2+x^2-2xL}} - h+x+\frac{2xhL-x^2h+h(L-x)\sqrt{n^2L^2+x^2-2xL}}{L\sqrt{n^2L^2+x^2-2xL}}\right]. \tag{9}$$

From Eq. (9) and given values of n, h, and L, we have the form of OPD(x). Then, the fractional mode number of s-AFPF pass band center wavelength with actuator at position x is

$$m_s(x) = \frac{\mathrm{OPL}(x)}{w_s(x)} = \frac{\mathrm{OPL}(0)-\mathrm{OPD}(x)}{w_s(x)}, \tag{10}$$

where OPL(0) is the starting condition.

From Eq. (10), we can calculate the fractional mode number of s-AFPF pass band center wavelength when the actuator moves to any position from its initial position.

We have indicated that the s-AFPF in Fig. 7 has the same parameters with the s-AFPF air|(HL)^{7}H-2L-H(LH)^7|glass, and the incident light wave at the s-AFPF can be regarded as a TE plane wave. Hence, with the L of 81 mm, n of 1.5168, h of 2 mm, and OPL(0) of 449.9 mm, by Eq. (9), we can first ascertain OPD(x) — the change in external cavity round trip optical path length versus actuator displacement from its initial position. Then, by characteristic matrix method, we can ascertain $w_s(x)$ — the pass band center wavelength of s-AFPF versus actuator displacement from its initial position. At last, by Eq. (10), we can ascertain $m_s(x)$ — the fractional longitudinal mode number versus actuator displacement from its initial position.

Figure 9 gives the relationship between the pass band center wavelength of s-AFPF and its corresponding fractional longitudinal mode number, as beam incident angle at s-AFPF varies from 0° to 37°. From Fig. 9, we find the fractional longitudinal mode number of the pass band center wavelength of s-AFPF increases first and then de-

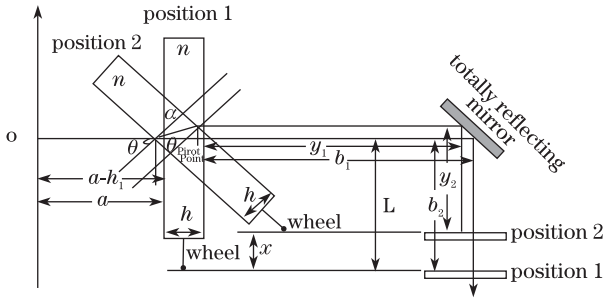

Fig. 8. Schematic diagram on how external cavity optical path varies as the actuator pushes forward from its initial position

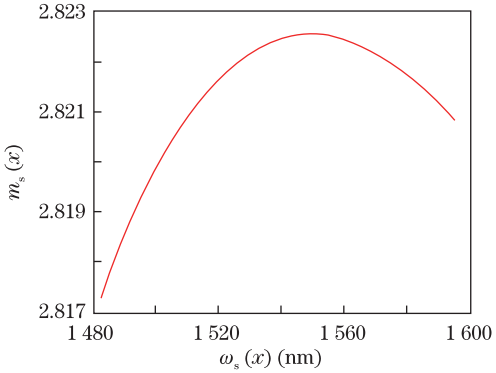

Fig. 9. $\omega_s(x)$ versus $m_s(x)$

creases as the actuator pushes forward from the initial position. There is only a limited flat region, in which the fractional longitudinal mode number can keep unchanged. It shows us that only in this region, the pass band center wavelength of s-AFPF for TE polarized light can have a synchronous variation with the wavelength of a fixed external cavity longitudinal mode, and this region is thus called the mode-hop-free wavelength tuning region. Here, the mode-hop-free wavelength tuning region covers a range of 1 547.2—1 552.6 nm, the corresponding actuator displacement from the initial position is 5.9—6.7 mm, and the locked and output external cavity longitudinal mode number is 282, 254. In this region, the theoretical value of the actuator displacement from its initial position, the pass band center wavelength of s-AFPF, and its corresponding fractional longitudinal mode number are given in Table 1.

From Table 1, we can see the fractional longitudinal mode number varies from 282, 253.8 to 282, 254.4, and then back to 282, 253.6, the external cavity will be lasing reliably on longitudinal mode 282, 254, giving mode-hop-free performance over the approximate wavelength range from 1 552.6 to 1 547.2 nm. The corresponding actuator displacement is approximately from 5.90 to 6.66 mm.

In conclusion, we investigate the transmittance characteristics of s-AFPF with the characteristic matrix method. In a certain range there is a quasi-linear relationship between the optical intensity peak-transmittance wavelength of s-AFPF and the cosine value of TE or TM plane wave incident angle at s-AFPF. Based on this feature, we propose a configuration with a s-AFPF in a tunable ECDL, which is able to make the cosine value of plane wave incident angle at s-AFPF have a quasi-linear variation with the ECDL external cavity round trip optical path length. By theoretical calculation, this configuration can achieve quasi-linear wavelength tuning over about a 5-nm range centered at about 1 550 nm without mode hops. To further improve the performance of this ECDL configuration, we should ensure that the incident angle of the collimated laser beam at s-AFPF is not too large.

Table 1. The theoretical Value of the Actuator Displacement from its Initial Position, the Pass Band Center Wavelength of S-AFPF, and its Corresponding Fractional Longitudinal Mode Number in the Mode-hop-free Wavelength Tuning Region

x (mm)	$w_s(x)$ (nm)	$m_s(x)$
5.898108	1 552.6	282 253.8
6.004483	1 551.9	282 254.1
6.111771	1 551.1	282 254.3
6.219972	1 550.3	282 254.4
6.329085	1 549.6	282 254.3
6.439107	1 548.8	282 254.2
6.550038	1 548.0	282 254.0
6.661875	1 547.2	282 253.6

This work was supported by 2009 Shenzhen Technology Research and Development Fund (No. O702011001) and 2010 Guangdong—Chinese Academy of Sciences Comprehensive Strategic Cooperation Project (No. 2010A090100014).

References

1. C. Ye, *Tunable External Cavity Diode Lasers* (World Scientific, Singapore, 2004).
2. M. de Labachelerie and G. Passedat, Appl. Opt. **32,** 269 (1993).
3. M. Bagley, R. Wyatt, D. J. Elton, H. J. Wickes, P. C. Spurdens, C. P. Seltzer, D. M. Cooper, and W. J. Devlin, Electron. Lett. **26,** 267 (1990).
4. H. Tabuchi and H. Ishikawa, Electron. Lett. **26,** 742 (1990).
5. F. Favre, D. Le Guen, J. C. Simon, and B. Landousies, Electron. Lett. **22,** 795 (1986).
6. F. Favre and D. Le Guen, Electron. Lett. **27,** 183 (1991).
7. L. Levin, Opt. Lett. **27,** 237 (2002).
8. K. Liu and M. G. Littman, Opt. Lett. **6,** 117 (1981).
9. I. Shoshan, N. N. Danon, and U. P. Oppenheim, J. Appl. Phys. **48,** 4495 (1977).
10. M. G. Littman and H. J. Metcalf, Appl. Opt. **17,** 2224 (1978).
11. P. McNicholl and H. J. Metcalf, Appl. Opt. **24,** 2757 (1985).
12. R. P. Salathe, Appl. Phys. **20,** 1 (1979).
13. M. G. Boshier, D. Berkeland, E. A. Hinds, and V. Sandoghdar, Opt. Commun. **85,** 355 (1991).
14. T. Hidaka and T. Nakamoto, Electron. Lett. **25,** 1320 (1989).
15. G. A. Coquin and K. W. Cheung, Electron. Lett. **24,** 599 (1988).
16. J. R. Andrews, Opt. Lett. **16,** 732 (1991).
17. G. Greiner, B. Boggs, T. Wang, and T. W. Mossberg, Opt. Lett. **23,** 1280 (1998).
18. H. A. Macleod, *Thin-Film Optical Filters* (Institute of Physics, London, 1999).